Seismic performance of existing tunnels affected by lining thickness reduction

Connecting Communities Through Underground Infrastructure – Eberhardt et al. (Eds)

Seismic performance of existing tunnels affected by lining thickness reduction

D. Boldini, E. Lusini and C. Spaggiari
Sapienza University of Rome, Rome, Italy

A. Carigi, C. Todaro and D. Peila
Politecnico di Torino, Turin, Italy

ABSTRACT: The ageing of post-war underground transport infrastructures is raising increasing concerns, as many tunnels were built without seismic design provisions and now exhibit significant signs of structural degradation. This study investigates the seismic vulnerability of road tunnels affected by reductions in lining thickness at the crown – a condition frequently reported during recent inspections. A typical two-lane tunnel with a 50 cm thick unreinforced lining, without an invert arch, was analysed as an example to define the potential criticality of this defect. Residual thicknesses of 20 cm and 10 cm were considered, assuming a good-quality rock mass (GSI = 65) and two overburden scenarios equal to two and four times the tunnel diameter. The soil-structure interaction problem was addressed through 2D finite element analyses under plane strain conditions, with an equivalent shear strain increment applied to simulate seismic loading. The lining was modelled using elastic and no-tension laws, while the ground was represented as elastic-perfectly plastic with a Mohr-Coulomb criterion. The results indicate that localised crown thinning significantly increases lining vulnerability under seismic loading, leading to critical stress conditions. These findings confirm the need for targeted evaluation methods and maintenance interventions to ensure the safety and resilience of ageing tunnels.

1 INTRODUCTION

The maintenance and safety assessment of existing tunnels are fundamental steps in infrastructure management and require a structured and standardised approach to ensure resilience and regulatory compliance.

After the Second World War, Italy's complex orography led to the construction of numerous road and railway tunnels, many of which are now nearing the end of their design life after over 70 years of service. With more than 9,000 tunnels extending for about 2,600 km across the national territory, managing this vast asset poses a major challenge within an increasingly extensive and ageing road network. To address these challenges, Italian tunnel maintenance regulations have evolved over time, culminating in 2022 with the issuance of the "*Italian Guideline for the Risk Classification, Safety Evaluation, and Monitoring of Existing Tunnels"* by the Italian Superior Council of Public Works, a body of the Ministry of Infrastructure and Transport (MIMS). This guideline provides a unified methodology to assess risk, ensure safety, and plan maintenance operations on a national scale, and is a mandatory reference for road and highway tunnel owners across Italy. Following the implementation of these regulations, a systematic assessment of infrastructure conditions has been carried out across the

DOI: 10.1201/9781042001064-625

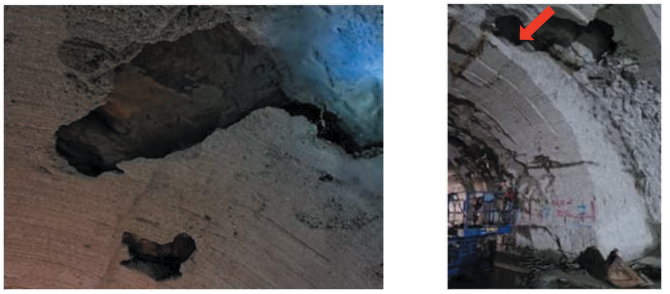

Figure 1. Examples of defects in tunnel lining with reduced thickness, identified during the refurbishment of the Monte Bianco Tunnel in Italy, after milling approximately 25–30 cm of the lining with a roadheader (courtesy of Traforo del Monte Bianco GEIE).

Italian highway network, based on site inspections, ground-penetrating radar surveys (to assess lining thickness or void presence), core drilling (to assess concrete strength), and stress measurements in the linings (Carigi et al. 2025). With this extended surveying on more than 1000 of tunnels, various types of defects have been observed, such as fissures, gravel nests, and voids mainly located at the lining extrados in the tunnel crown (Alessio et al. 2024).

The present research highlights growing concerns linked to two key factors: seismic action, not considered in the original 1960s-1970s designs, and the reduced lining thickness in the crown area, often associated with the construction techniques and concrete casting procedures used at the time. These techniques – ranging from conveyor belts to pneumatic impulse pumps – combined with limited vibration and low-quality concrete, led to the defects currently observed in the linings. During the inspections, many voids or incomplete filling of the excavation profile were observed in the tunnel crown, producing linings of irregular thickness or with sections not fully in contact with the rock mass. The stability of these geometries was, anyway, ensured over the tunnel's lifetime as the stress state in the lining is usually very low: in about 90% of the very large number of measurements carried out in Italian highway tunnels the values could be reconducted to the self-weight of the lining. As an example, Figure 1 shows a case of reduced lining thickness and voids at the tunnel extrados, discovered during the development of refurbishment works for the Monte Bianco Tunnel in Italy, which was opened to traffic in 1962.

2 INVESTIGATED SCENARIOS

The research goal is to understand if the combination of the reduced lining thickness and the seismic action for tunnels excavated in rock masses is a problem that requires further investigation and structural countermeasures. The analyses were conducted using a lining geometry and thickness typical of road tunnels excavated in rock masses in Italy during the 1960s–1970s. The construction practices and geometrical characteristics typically adopted at the national level during that period did not include an invert and relied on a limited number of steel arches and/or rock bolts. The investigated configuration consists of a horse-shoe shape section with an external diameter of 12.3 m and a 50 cm thick unreinforced concrete lining and was obtained, as a schematic example, from the original design of many tunnels of the considered construction time (Figure 2). Two overburden depths, H, were considered, equal to two and four times the tunnel diameter ($2D$ and $4D$), a frequent condition observed for example in the highway running along the Ligurian sea.

A good-quality, undisturbed rock mass was considered, and its parameters were derived from the properties of a representative intact rock, following the empirical approach proposed by Hoek et al. (2002). A Geological Strength Index (GSI) of 65 and a disturbance factor D_f = 0 were assumed. Additional properties of the rock mass included a unit weight g_r = 25.0 kN/m^3 and Poisson's ratio of ν_r = 0.35. The intact rock and the resulting rock-mass properties are

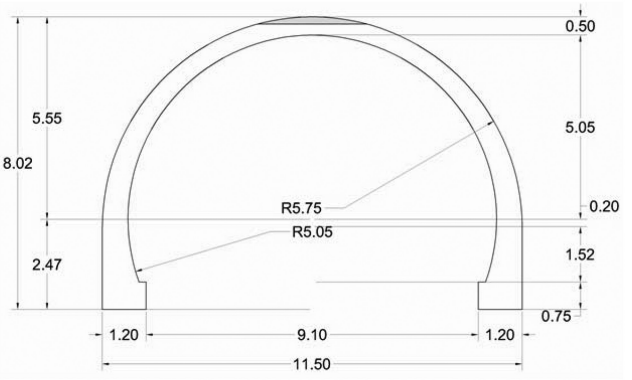

Figure 2. Typical road tunnel cross-section considered in the analyses (dimensions are in m).

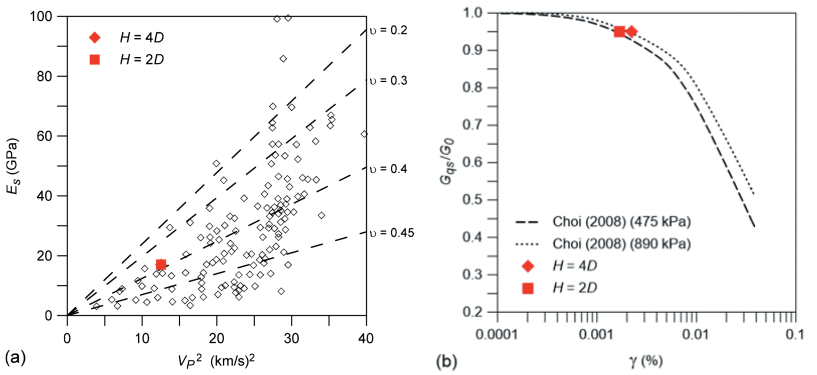

Figure 3. (a) Comparison of the assumed material with typical Italian rock-masses in terms of dependency of the static elastic modulus on the squared P-wave velocities at given Poisson's coefficient (Ribacchi 1987). (b) Shear stiffness decay curve, showing the operational shear stiffness and the maximum shear strain representative of seismic actions at tunnel depth.

summarised in Table 1. The strength parameters obtained from the Hoek-Brown criterion were subsequently linearised according to the Mohr-Coulomb failure model. Equivalent shear strength parameters of $\varphi' = 59°$ and $c' = 1.325$ MPa were adopted for both overburden scenarios. The Young's modulus of the rock-mass in static conditions E_s was estimated from the intact rock modulus E_i using the formula proposed by Hoek & Diederichs (2006). Once rock-mass modulus in static conditions was defined, an adequate value of the small-strain stiffness parameters was attempted with a trial-and-error procedure based on empirical evidence for Italian rock-masses (Ribacchi 1987) (Figure 3a).

To evaluate the influence of structural degradation and construction-related defects on the seismic response of the tunnel, several configurations with reduced lining thickness at the crown were analysed. Starting from the nominal thickness of 50 cm, the crown section was reduced to 20 cm and 10 cm, simulating voids behind the lining. This range of reductions reflects conditions typically observed during recent inspections of existing tunnels (see Figure 1). The adopted material corresponds to a C16/20 concrete, representative of values obtained from tests on cores from existing tunnel linings extracted during refurbishment works. The corresponding mechanical parameters are given in Table 2 according to Eurocode 2 (EN1992-1-1:2023), with an unreinforced concrete unit weight of $g_c = 24.5$ kN/m^3.

A value of peak ground acceleration $PGA = 0.35$ g was assumed at the outcrop to represent a severe seismic scenario. The seismic action at tunnel depth was evaluated in accordance with

Table 1. Intact rock and rock-mass parameters.

Intact rock		Rock-mass	
Uniaxial compressive strength σ_{ci}	70 MPa	Uniaxial compressive strength σ_{ca}	9.94 MPa
Material constant m_i	10	Tensile strength σ_{ta}	-0.50 MPa
Young's modulus E_i	27 GPa	Young's modulus E_s	17.06 GPa

Table 2. Characteristics of the concrete lining (C16/20) according to Eurocode 2 (EN1992-1-1:2023).

Characteristic cylindrical compressive strength f_{ck}	16 MPa
Mean cylinder compressive strength f_{cm}	24 MPa
Mean tensile strength f_{ctm}	1.9 MPa
Young's modulus E_c	28.6 GPa
Poisson's ratio ν_c	0.2

the procedure described in the proposed second generation of the Eurocode 8, Part 5, Annex G (prEN 1998-5:2024). The maximum shear stress τ_{max} at the tunnel axis depth z_t was obtained from the equilibrium of horizontal forces acting on a soil column of unit width:

$$\tau_{max} = \left(\frac{PGA}{g}\right)\sigma_v r_{dt} \tag{1}$$

where g is the gravity acceleration and σ_v is the total vertical stress. The depth-dependent stress reduction function r_{dt} can be calculated as:

$$r_{dt} = \begin{cases} 1.0 & z_t < 10\text{m} \\ 1.2 - 0.02z_t & 10 \leq z_t < 35\text{m} \\ 0.5 & 35\text{m} \leq z_t \end{cases} \quad \text{with } z_t = H + \frac{D}{2} \tag{2}$$

To assess the values of the shear stiffness G_{qs} and $\gamma_{max} = \tau_{max}/ G_{qs}$ compatible with the seismic event, an iterative procedure was applied adopting the laboratory-scale shear stiffness decay curve for intact tuff rock from Choi (2008) (Figure 3b). Although not strictly representative of rock masses, these curves were adopted due to the lack of validated alternatives at the rock-mass scale; moreover, their explicit dependence on the confining stress allowed the in-situ stress state to be accounted for, thus differentiating between the $2D$ and $4D$ overburden scenarios.

The maximum expected shear strain, γ_{max}, was 0.00168% and 0.00224% for $2D$ and $4D$, respectively. The corresponding Young's moduli, E_{qs}, were equal to 18.89 GPa in both cases.

3 NUMERICAL APPROACH

The soil-structure interaction problem was addressed through 2D finite element analyses developed in Plaxis 2D, considering a tunnel cross-section under plane strain conditions following the simplified procedure introduced by Kontoe et al. (2008) in which seismic loading was simulated by an equivalent shear strain increment. The plane strain assumption was adopted as a first-order simplified approach, conservatively assuming an indefinite out-of-plane extension of the crown void and allowing a preliminary assessment of the tunnel-ground interaction under seismic actions. This idealisation necessarily neglects aspects such as the finite extent of the defect in the out-of-plane direction, the combination of axial and shear

seismic actions, ground inertial effects, site-specific stratigraphic amplification, and cyclic degradation of material properties.

The lining was modelled using both elastic (Linear Elastic, LE) and no-tension (Elasto-Plastic, EP) constitutive laws, while the rock-mass was represented as an elastic-perfectly plastic material, following the Mohr-Coulomb failure criterion, with stiffness values consistent with the strain levels developed during the various calculation stages, as described in the previous section.

Figure 4a,b and c illustrate the computational mesh adopted for the 4*D* overburden scenario. The lining was modelled using volume elements, partially not activated to simulate the three cases of reduced thickness. An elasto-plastic interface was defined between the rock-mass and the lining, with strength parameters reduced to the 70% of those of the rock-mass and a zero tensile strength.

The implemented calculation stages are illustrated as follows. After initialising the in-situ stress state (K_0 = 0.5), tunnel excavation was simulated by deactivating the elements within the excavation section and applying a stress release factor, λ, of 90%. The lining was then activated and λ was increased to 100%. Finally, the quasi-static phase consisted of applying a shear strain, γ_{max}, to the computational domain. For the first three static phases, the rock mass stiffness was set equal to E_s. For the fourth quasi-static phase, the stiffness was varied and set equal to E_{qs}.

The boundary conditions were defined in terms of displacements, fully fixed at zero at the base of the model and restrained in the horizontal direction along the lateral boundaries. During the quasi-static phase, a horizontal displacement of $u_{max} = \gamma_{max} \cdot Z$ was applied along the top boundary. Horizontally varying displacements, increasing linearly from 0 to u_{max}, were applied along the lateral boundaries.

The axial forces and bending moments developed in the lining were subsequently compared with the *N-M* interaction domains of various lining sections, showing that failure conditions were approached in specific cases. The *N-M* interaction domains were calculated using the fibre method, adopting a parabolic stress-strain law for concrete based on its characteristic compressive strength. The tensile strength of the concrete was neglected, and no reduction coefficients were applied. For each analysed section, the domains were derived according to the local lining thickness, assuming the neutral axis position to be located at the mid-depth of the section and neglecting the slight curvature.

4 NUMERICAL RESULTS

Three configurations were analysed: the full section and two most critical cases with residual lining thicknesses (20 cm and 10 cm), considering both a linear-elastic (LE) and an elasto-plastic no-tension (EP) case. The 4*D* overburden case was selected for discussion, as it

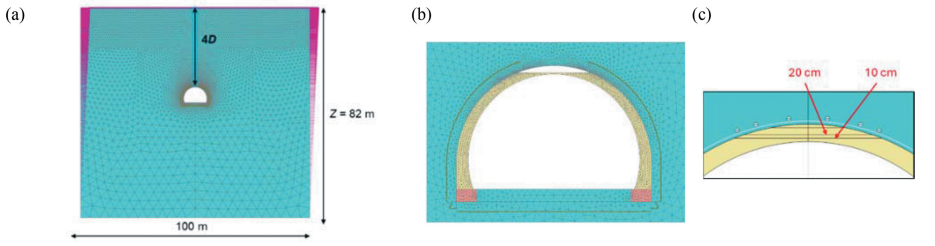

Figure 4. (a) Computational mesh for the 4*D* overburden scenario; (b) lining detail showing the maximum thickness reduction; (c) predefined cluster borders of the two residual thicknesses (10 and 20 cm).

exhibited greater deformations and higher structural demand compared to the 2*D* overburden scenario.

The numerical results are shown in terms of deformed shapes to illustrate the behaviour of the lining subjected to shear strain induced by seismic actions applied in a quasi-static manner (Figure 5). In the linear-elastic cases (Figure 5a-c), the imposed shear strain induces the opening of a gap between the soil and the lining at the top-left corner near the crown. In addition, a second gap develops near the bottom-right sidewall, accompanied by a slight uplift of the ground profile. The normal force and bending moment diagrams (Figure 6) confirm these observations: for all analysed sections, the left sidewall remains under compression, while the axial forces tend to zero near the right sidewall. The gap propagation towards the pre-existing void induces a noticeable inflection of the remaining lining slab. This behaviour is reflected in the bending moment distribution: on the left side, the lower fibres are in tension (negative moment according to the adopted convention), while towards the crown, the moment progressively decreases to zero and then changes sign, inducing tension in the upper fibres near the area of reduced thickness. On the left side of the crown, the normal force decreases and becomes negative indicating the build-up of tensile forces out of the capacity of the section.

The elasto-plastic lining (Figure 5d-f) exhibits a similar overall deformation pattern but with smaller magnitudes. The gap at the top-left corner is less pronounced than in the linear-elastic case, and no detachment occurs at the right sidewall. Stress redistribution is confirmed by the absence of tensile forces which are bounded by the tensile cut-off at the left haunch and the presence of a slight compression in the right sidewall (*N* diagram in Figures 6b,d,f). The bending moment diagrams also show lower peak values, indicating a less pronounced inflection at the crown (Figure 6). These results highlight the greater ductility and energy dissipation capacity of the elasto-plastic behaviour, which reduces stress concentration and limits gap formation compared to the linear-elastic response.

The internal force couples (*N*, *M*) obtained from both the static and quasi-static analyses are plotted against the corresponding *N*-*M* interaction domains. The plots include only the points corresponding to selected positions along the tunnel crown, defined in polar coordinates as the angle measured from the left sidewall. Results are presented for the full section (Figure 7) and for the 20 cm and 10 cm residual thicknesses (Figures 8 and 9, respectively).

The static condition is satisfied in all cases. In addition, the full section with the elasto-plastic lining also meets the requirement when considering the additional loading applied after the quasi-static phase (Figure 7b). For linings with reduced thicknesses of 20 cm and 10 cm, the verification at the tunnel crown remains fulfilled, although the *N*-*M* points lie close to the interaction domain boundary – at 70° and between 80° and 95° for the 10 cm case (Figure 8)

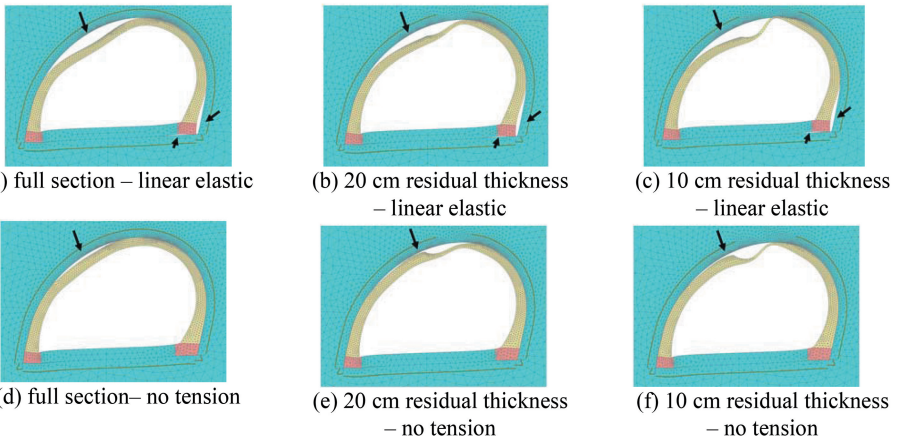

Figure 5. Deformed shapes scaled to 5,000 for full section (a,d), 20 cm (b,e) and 10 cm (c,f) crown thicknesses for linear elastic lining (LE, a-c) and no-tension (EP, d-f) for 4*D* overburden.

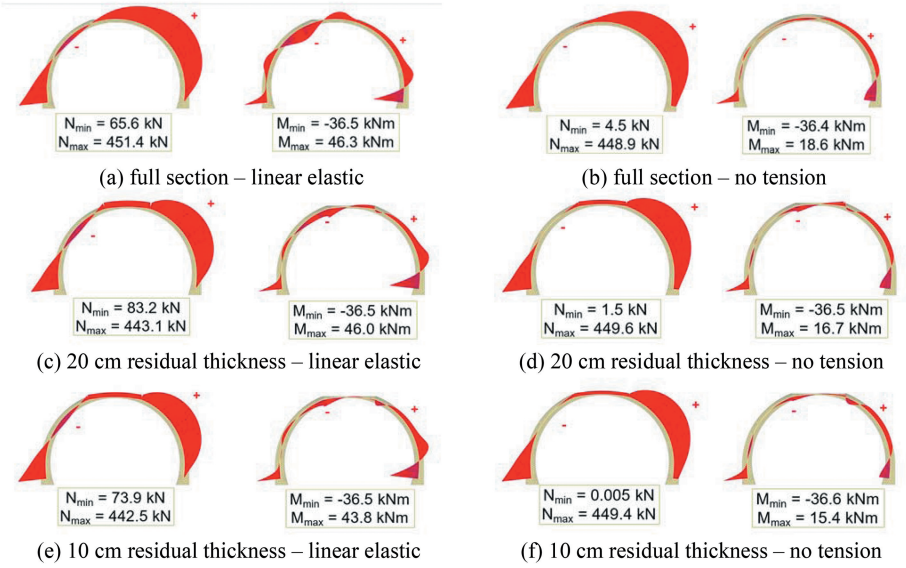

Figure 6. Normal force (N), scaled to 0.01, and bending moment (M), scaled 0.05, acting in the tunnel lining after the quasi-static phase for 4D overburden.

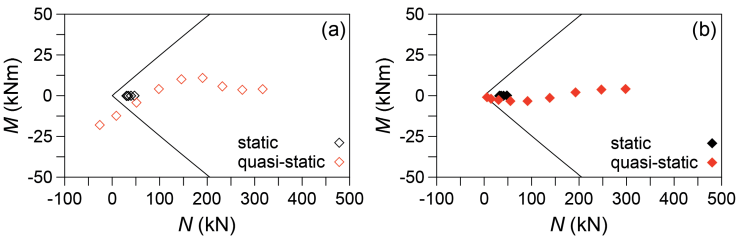

Figure 7. Full section (angular interval 70°-110°) for linear-elastic (a) and no-tension (b) linings under a 4D overburden, considering both the static and quasi-static phases.

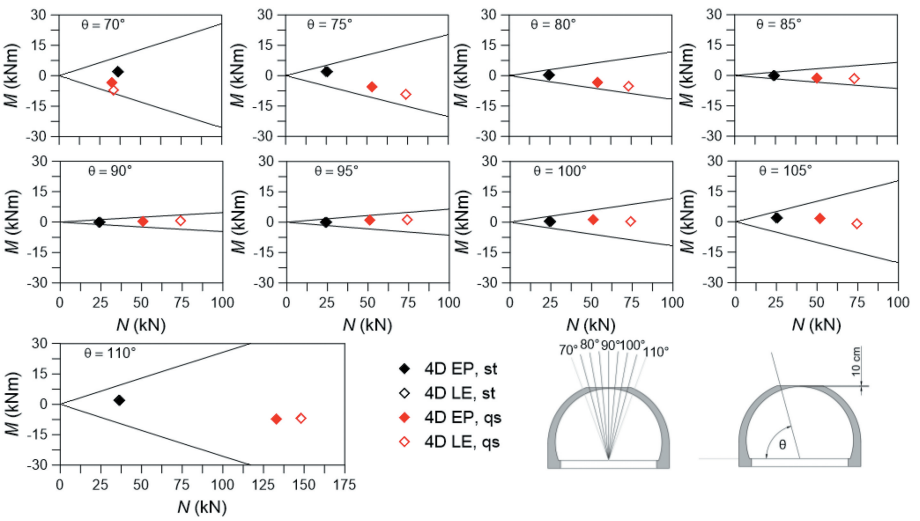

Figure 8. N-M interaction diagrams for 10 cm residual thickness in 4D overburden for static (st) and quasi-static (qs) loading for a linear-elastic (LE) and no-tension (EP) lining.

and at 85° for the 20 cm case (Figure 9). The induced forces are not verified only for the linear-elastic lining, specifically at the location corresponding to the change in thickness at approximately 70° on the left side of the tunnel crown. Owing to the low compressive stresses accumulated during the static phase, the quasi-static analysis produces unrealistic tensile stress distributions. Consequently, the elastic assumption for the lining behaviour, unlike what is typically acceptable for compressed sections, results in completely unreliable outcomes.

Figure 10 shows the distribution of plastic points for all analyses under a 4*D* overburden condition. For the linear-elastic lining, plastic points are concentrated along the ground-lining interface, where partial detachment was previously observed. As the lining thickness decreases, the plastic points at the ground-lining interfaces reduces proportionally to the length over which the detachment occurs. For the elasto-plastic lining notable differences in the extent and distribution of plastic points are observed. In this case, tensile cut-off points also develop within the lining itself, due to the tensile cut-off, distributing over a fan-shaped region starting approximately 30° from the left sidewall and extending towards the crown to about 100°. Additional cut-off points develop at the bottom-right sidewall where also the rock-mass and the interface reach the tensile strength locally. With reductions in lining thickness, the plastic zone expands towards to the right side of the crown, increasing the likelihood of instability at both ends of the crown slab and highlighting the progressive weakening of the tunnel section.

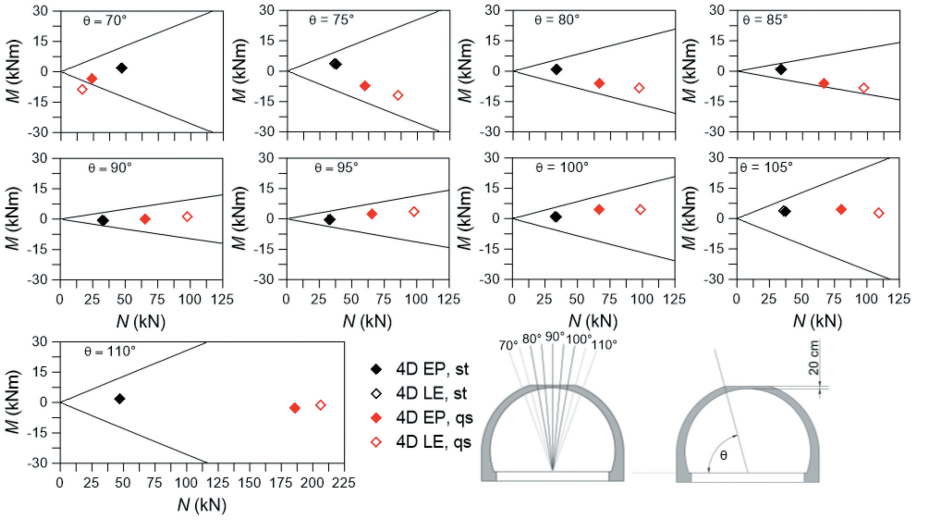

Figure 9. *N-M* interaction diagrams for 20 cm residual thickness in 4*D* overburden for static (st) and quasi-static (qs) loading for a linear-elastic (LE) and no-tension (EP) lining.

5 DISCUSSION AND CONCLUSIONS

The seismic response of differently damaged tunnel linings was analysed through 2D finite element simulations under plane strain conditions, applying an equivalent shear strain increment to simulate seismic loading derived using a simplified approach based on the procedures suggested in the Eurocode for scaling the *PGA,* adopted as 0.35 g at the outcrop to represent a severe seismic scenario. The results obtained assuming good-quality rock-mass (*GSI* = 65), two overburden scenarios (*H* = 2*D* and 4*D*), and lining models (linear-elastic and no-tension), indicate potential structural concerns related to the damage in the lining and at the rock-lining interface. Damage

concentrates at locations corresponding to thickness discontinuities near the crown, while possible block detachment in the unsupported zone above the crown slab may impose additional loads, potentially leading to local collapses.

The present analyses, relying on plane-strain quasi static assumptions, cannot account for advanced aspects of dynamic soil-structure interaction. However, they represent a simple, reproducible and effective tool for identifying the main critical issues related to excessive seismic-induced shear strain in common Italian tunnel lining geometries from the 1960s and 1970s, that are structurally unsound due to typical construction defects. Further analyses are required to refine the assessment and identify possible strengthening or rehabilitation strategies.

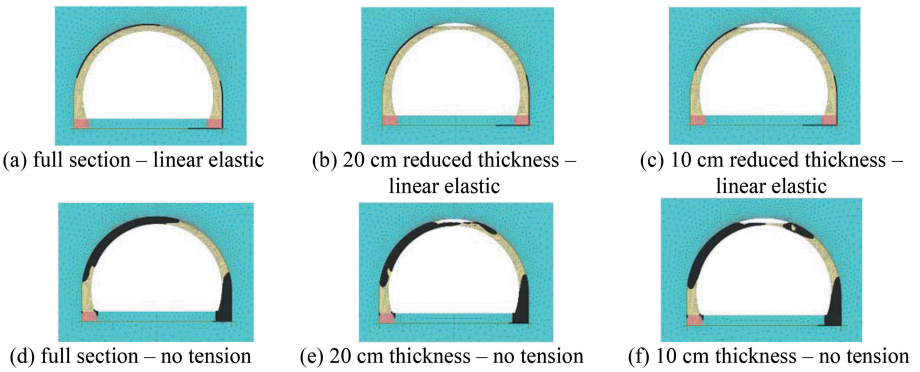

Figure 10. Plastic points distributions: black dots represent tensile cut-off points.

ACKNOWLEDGEMENTS

This work was carried out within the framework of the Research Project ArciTunLin: "Assessment, Risk Classification and Interventions on TUNnel LINings", funded by FABRE Consortium.

REFERENCES

Alessio, C., Baccolini, L., Di Fiore, D., Conte, M., Cicolani, M., Peila, D. & Carigi, A. (2024). The 365 km tunnels assessment along ASPI Motorways Network – Key findings addressing risk analysis procedures and structural conditions evaluation and strategy of interventions. *Procedia Structural Integrity, II Fabre Conference (FABRE24)*, 62: 1077–1088.

Carigi, A., Todaro, C. & Silvestri, G. (2025). Italian legislative scheme for tunnel maintenance up to the guidelines for the risk classification, safety evaluation, and monitoring of existing tunnels. *Geomechanics and Tunnelling* 18 (4): 312–319.

Choi, W.K. (2008). Dynamic properties of ash-flow tuffs. Ph.D. thesis, University of Texas, Austin, Texas.

Hoek, E., Carranza-Torres, C. & Corkum, B. (2002). Hoek-Brown failure criterion – 2002 Edition. In Hammah et al. (eds.), *Proc. of the 5th North American Rock Mech. Symp. and the 17th Tun. Ass. of Canada Conf. (NARMS-TAC 2002), Toronto, 7-10 July 2002*. University of Toronto Press, vol. 1, pp. 267-273.

Hoek, E. & Diederichs, M.S. (2006). Empirical estimation of rock mass modulus. *International Journal of Rock Mechanics & Mining Sciences* 43: 203–215.

Kontoe, S., Zdravkovic, L., Potts, D.M, & Menkiti, C.O. (2008). Case study on seismic tunnel response. *Canadian Geotechnical Journal* 45(12): 1743–1764.

Ribacchi, R. (1987). Rock mass deformability. In situ-tests, their interpretation and typical results in Italy. In *Proc. of Int. Symp. On Field Measurements in Geomechanics*, Kobev vol. 1, pp. 171–192.